# Possible origin of the 175 $cm^{-1}$ Raman mode in altermagnetic MnTe

Bishal Thapa [1,2] K. D. Belashchenko [3] and Igor I. Mazin [1,2]
[1]*Department of Physics and Astronomy, George Mason University, Fairfax, Virginia 22030, USA*
[2]*Quantum Science and Engineering Center, George Mason University, Fairfax, Virginia 22030, USA*
[3]*Department of Physics and Astronomy and Nebraska Center for Materials and Nanoscience, University of Nebraska-Lincoln, Lincoln, Nebraska 68588, USA*

(Received 15 February 2026; revised 10 July 2026; accepted 15 July 2026; published 11 August 2026)

MnTe has recently attracted exceptional attention due to its well-established altermagnetism, prompting a thorough reexamination of its properties. In particular, it was found that a Raman-active excitation at ∼175 $cm^{-1}$, routinely assigned to the $E_{2g}$ phonon, is incompatible with this interpretation. It was further hypothesized that this mode is a "leakage," due to symmetry lowering, of an otherwise forbidden phonon. Here, using first-principles calculations, we decisively rule out this hypothesis and propose an alternative interpretation that the "mystery mode" is an electronic excitation, i.e., a plasmon, enabled by hole self-doping. The resolution of this mystery will require additional experiments and could shed new light on the nature of electronic transport in MnTe.

DOI: 10.1103/7pd9-xwmw

## I. INTRODUCTION

MnTe has gained a lot of attention recently. Arguably, it is the best studied altermagnetic material, with 25 papers published and 47 preprints posted just in 2025 (see Ref. [1], and references therein). One of the reasons for the broad scientific appeal of MnTe is its perceived simplicity. However, as discussed in this paper, there is a completely unresolved and not understood issue related to its Raman spectrum, which may have important ramifications for its electronic structure and transport properties.

Despite intense interest in MnTe, only a handful of Raman studies have been published [2–7], as summarized in Table I. While all papers report a Raman mode around 170–200 $cm^{-1}$, the results are somewhat contradictory in terms of the exact frequency, temperature variation, and polarization dependence. In this respect, the recent preprint of Wu *et al.* [7] stands out. While previously this mode had been assigned to the $E_{2g}$ phonon (the only one allowed by symmetry), they pointed out that density-functional theory (DFT) calculations place this phonon below 100 $cm^{-1}$. Such an error is highly unusual in DFT, especially in such a simple material. In Ref. [7] the calculated frequency was 83 $cm^{-1}$; we have verified that varying input parameters, such as the Hubbard $U$, or changing the density functional to metaGGA or hybrid ones, cannot raise this frequency to more than 100 $cm^{-1}$.

Furthermore, Wu *et al.* have also measured the polarization dependence and found the mode to be active only in the parallel polarization, while by symmetry [8] the $E_{2g}$ phonon should be equally active in both geometries. (This claim contradicts some earlier claims [3,4] based on thin films, which can probably be considered superseded by these more recent measurements.) At first glance, the ∼175 $cm^{-1}$ feature might be interpreted as a two-phonon process, since its energy is not far from twice the calculated $E_{2g}$ frequency. However, several arguments disfavor this assignment. First, the observed line is too narrow for a two-phonon signal, which samples finite-momentum phonons and is therefore usually broader. Second, a two-$E_g$-phonon process should also appear in cross polarization, contrary to the polarization-resolved data reported in Ref. [7]. Note that potential resonant effects are unlikely to account for the ∼175 $cm^{-1}$ feature appearing similarly across studies summarized in Table I, as Raman data in several of these works were obtained with different excitation wavelengths 514–633 nm (e.g., 532 nm in Ref. [6], 632.8 nm in Ref. [5], and 633 nm in Ref. [7]).

Overall, Ref. [7] makes a convincing case against the assignment of the 175 $cm^{-1}$ mode to the $E_{2g}$ phonon. In addition, a report of a coherent pump-probe excitation at this frequency in Ref. [9] also casts doubt on its $E_g$ symmetry: within the displacive excitation of coherent phonons (DECPs) mechanism [10], normally only $A_1$ modes can be coherently excited, not $E_g$ modes

This raises the question: What is it then? A leakage of modes forbidden by symmetry or by momentum conservation is highly unlikely, since it would require a large concentration of symmetry-breaking defects, and is not expected to produce a single narrow linebecause all momenta contribute to such leakage. Given that 120–140 $cm^{-1}$ modes are traditionally associated with Te precipitates [4], one may think of another precipitate phase, which we will discuss later. Reference [7] proposes an interesting, albeit probably incorrect, as we argue later in this paper, scenario: they suggest that the experimentally well-established crystal structure of the space group $P6_3/mmc$ (No. 194) is incorrect, and in reality the Mn planes are alternatively shifting up and down along $c$ by $\delta \sim \pm 0.001c \approx 0.007$ Å, which is 20 times smaller than the zero-point motion amplitude for this mode. While Wu *et al.* correctly point out that in the resulting space group, $P\bar{6}m2$ (No. 187), the originally silent $B_{1u}$ mode becomes Raman active (but not in the cross polarization), they missed the point that the acquired activity is proportional to $\delta^2$, so likely negligibly small.

In the following, we carefully verify this hypothesis by (i) fully optimizing the DFT crystal structure, and showing

 

TABLE I. Reported frequencies of the Raman mode in the 170–200 $cm^{-1}$ range in MnTe from the literature. The column "note" distinguishes thin films, bulk samples, and single crystals (denoted as "Xtal"). The column "polarization" lists the scattering geometries in which the mode was reported; "–" indicates that no polarization-resolved Raman analysis was reported in the corresponding reference. The entry marked by * shows the frequency of a coherent phonon extracted from pump-probe measurements.

| $\omega$ ($cm^{-1}$) | $T$ (K) | Polarization | Ref. | Note | Year |
|---|---|---|---|---|---|
| ∼178 | 320 | – | [2] | bulk | 1985 |
| ∼187 | 100 | – | | | |
| ∼215 | 27 | *XY* only | [3] | film | 1997 |
| 195–197 | 25 | *XX* or *XY* | [4] | film | 2014 |
| ∼175 | 360 | – | [5] | film | 2020 |
| ∼177 | 200 | – | | | |
| ∼167 | 310–360 | – | [6] | Xtal | 2024 |
| ∼170 | 240 | – | | | |
| ∼175 | RT | *XX* only | [7] | Xtal | 2025 |
| ∼175 | 320 | | [9] | Xtal | 2021 |
| ∼178 | 77 | * | | | |

that it invariably converges to the $P6_3mmc$ structure, and (ii) by calculating, using the Placzek formula [11], the Raman activity, and showing that it is negligibly small. We further suggest another explanation, that the mode in question is in fact a plasmon excitation of the self-doped holes. We calculate the plasmon frequencies in DFT and show that they are in the right frequency range. Note that plasmon is only Raman active in the *XX* polarization, in agreement with the experiment in Ref. [7].

It remains to be seen why the plasmon frequency (if it is one) is relatively robust from sample to sample. In Table II we summarized reported measurements of the hole concentration $n$. There are some outliers, which also contradict each other, but in general for the stoichiometric MnTe $n \sim (2\text{–}6.8)\times 10^{18}$, indicating a variation in $\omega_p$ by ±30%, while the frequency of the mode in question at room temperature (RT) varies between different experiments by less than 4%. One possible explanation is that $\omega_p$ is a direct probe of carrier density, regardless of the transport relaxation time, while the Hall coefficient can be dramatically affected by different bands crossing the Fermi level having different relaxation rates, plus can be contaminated by anomalous Hall conductivity.

If our proposal is confirmed by experiment, it will open up another window into the so far poorly understood origin of this hole doping; in particular, why the doping level appears to be rather stable between different samples.

TABLE II. Available data on the carrier concentration.

| $n$ ($10^{18}$ $cm^{-3}$) | $T$ (K) | Method | Ref. | Note | Year |
|---|---|---|---|---|---|
| 50 | 77–400 | Hall | [12] | bulk | 1964 |
| 0.04 | ∼0 | Hall | [13] | bulk | 2014 |
| 2 | 310 | | | | |
| 6.8 | RT | Hall | [14] | bulk | 2016 |
| 3.2 | RT | Hall | [15] | bulk $Mn_{1.06}Te$ | 2016 |
| <10 | 300 | Hall | [16] | bulk | 2017 |
| 6 | ∼0 | Hall | [17] | film | 2016 |

## II. FORBIDDEN-PHONON HYPOTHESIS

As discussed above, Wu *et al.* [7] proposed that the true crystal structure belongs to the lower symmetry group $P\bar{6}m2$ (No. 187) rather than the commonly reported $P6_3/mmc$ (No. 194). In this scenario, small alternating displacements of the Mn planes along the $c$ axis (by $\delta = \pm 0.1\%c$) are conjectured to render the otherwise silent $B_{1u}$ mode Raman active, potentially explaining the observed peak.

We have tested this hypothesis in two different ways. The first was to check whether DFT calculations starting with the proposed structure, converge to a structure with a finite $\delta$, or to a $\delta = 0$, within the numerical accuracy. We found the latter to be the case, for calculations fully converged in both $k$-points mesh and cutoff energy, regardless of the value of $U$ in DFT + $U$, of the pseudopotentials or the DFT flavor used (we checked local, gradient-corrected, and a hybrid functional).

Next, we calculated the Raman activity of the $E_{2g}$ mode as well as the initially forbidden $B_{1u}$ mode using the structure suggested in Ref. [7], even though it was not the lowest-energy structure in the calculations. We employed the Placzek formalism [11] to compute the Raman efficiency directly from DFT.

Within the Placzek approximation, the Raman efficiency of a phonon mode is given by [11,18]

$$S_{is}(\omega) = V(4\pi)^2\left(\frac{\omega}{c}\right)^4\left|\frac{\partial\varepsilon_{is}(\omega)}{\partial Q}\right|^2, \tag{1}$$

where $V$ is the unit cell volume, $\omega$ is the incident photon frequency, $c$ is the speed of light, and $Q$ is the normal coordinate of the phonon mode. The indices $i$ and $s$ denote the polarizations of the incident and scattered light. $\frac{\partial\varepsilon_{is}(\omega)}{\partial Q}$ is the measure of how the phonon displacement modulates the macroscopic dielectric response.

Several features of Eq. (1) can be summarized as follows. (1) The $(\omega/c)^4$ prefactor reflects the familiar wavelength dependence of light scattering. (2) The Raman activity is entirely encoded in $|\partial\varepsilon/\partial Q|^2$; a mode that does not modulate the dielectric tensor is Raman silent. (3) The polarization indices enforce symmetry selection rules: certain modes appear only for specific incident-scattered polarization combination. (4) For a mode that becomes active only through a small symmetry-breaking distortion $\delta$, the derivative $\partial\varepsilon/\partial Q$ itself scales as $\delta$, leading to an intensity scaling as $\delta^2$. By computing $\partial\varepsilon/\partial Q$ for the $B_{1u}$ derived mode in the $P\bar{6}m2$ structure (see Fig. 1) as a function of $\delta$, we can quantitatively assess whether the proposed symmetry lowering can produce a measurable Raman intensity.

First-principles calculations were performed within DFT using the Vienna *ab initio* simulation package [19–21]. The Generalized gradient approximation (GGA) [22] functional was used. On-site electronic correlations in Mn $3d$ states were taken into account using the DFT + $U$ method, with an effective Hubbard parameter $U_{\text{eff}} = 2.0$ eV. Varying or even eliminating $U$ did not lead to a qualitative change in the results.

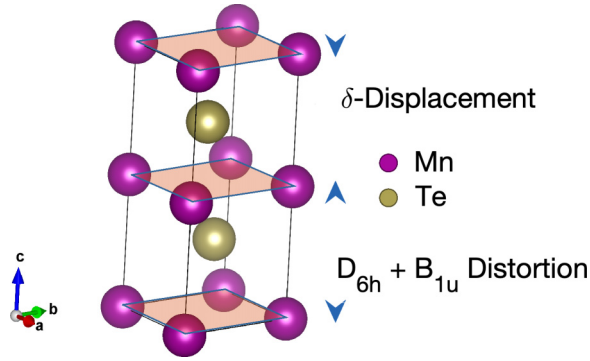


FIG. 1. Symmetry lowering $B_{1u}$ mode applied to parent $P6_3/mmc$.

A plane-wave cutoff was 540 eV, and a Γ-centered $10 \times 10 \times 6$ $k$-point mesh was used. Spin-orbit coupling was not included in the final calculations, as it was found to have a very small effect on the phonon frequencies or dielectric functions in the relevant frequency range.

Starting from the parent $P6_3/mmc$ (No. 194) structure, a $B_{1u}$ symmetry-breaking lattice distortion was frozen to obtain a reduced-symmetry $P\bar{6}m2$ (No. 187) as shown in Fig. 1. The phonon eigenvectors $\mathbf{e}_n$ and frequencies $\omega_{\rm ph}$ (Table III) of this structure were obtained using density-functional perturbation theory. Mode symmetries and selection rules were determined using the isotropy software suite [23,24].

To test whether the symmetry-breaking distortion proposed in Ref. [7] produces measurable Raman activity, we constructed $P\bar{6}m2$ (No. 187) structures for various $\delta$. For each structure the Raman tensor elements were evaluated by displacing atoms along the phonon eigenvector and computing the induced change in the macroscopic dielectric tensor, with atomic displacements $\mathbf{u}_n = \Lambda\,\mathbf{e}_n$, where $\mathbf{e}_n$ is the normalized phonon eigenvector for atom $n$. The displacement amplitude $\Lambda$ was chosen as $\Lambda = A_{\rm max}/e_{\rm max}$, with $A_{\rm max} = 0.02$Å, ensuring numerical accuracy of the finite-difference derivative.

The Raman tensor elements were then obtained by numerical differentiation of the dielectric function $\varepsilon_{\alpha\beta}(\omega_L)$ where $\omega_L$ is the laser frequency ($\hbar\omega_L = 1.96$ eV).

For each distorted structure a self-consistent electronic calculation was first performed to obtain the charge density, followed by a non-self-consistent optical calculation with `LOPTICS =.TRUE.` on a highly refined $k$ mesh.

The normal-coordinate mode amplitude $Q$ was defined, using atomic units, as usual, as $\mathbf{u}_n = \Lambda\mathbf{e}_n$ was taken as

$$Q = \Lambda\sqrt{2\omega_{\rm ph}}\sum_n \sqrt{M_n}\,\|\mathbf{e}_n\|^2, \tag{2}$$

where $\omega_{\rm ph}$ is the phonon frequency and $M_n$ are the atomic masses.

The results are summarized in Fig. 2 and in Table IV (the calculated frequencies are presented in Table III). We see that the Raman intensity of the $A_1'$ mode is nearly two orders of magnitude weaker than that of the $E'$ (or $E_{2g}$ in the original structure) and not that much larger than the calculated intensity of the same mode in the $zz$ polarization, where it is forbidden by symmetry. Thus, we can conclude, with confidence, the distortion-induced activity is way too weak to explain the experimentally observed mode at ∼175 cm$^{-1}$.

## III. IMPURITY PHASE HYPOTHESIS

It has been suggested [25,26] that the ∼175 cm$^{-1}$ mode is associated with the $MnTe_2$ precipitate phase, which does have an $A_{1g}$ phonon in the appropriate frequency range. There are now serious experimental arguments in favor of such an impurity-phase assignment, including Raman and diffraction measurements on samples containing $MnTe_2$-related secondary phases [27]. Nevertheless, as attractive as this hypothesis may be, it remains at odds with reports that the 175 cm$^{-1}$ feature in Refs. [5,6] is sensitive to the magnetic order in the MnTe host, as reflected by the anomalies near $T_N \sim 310$ K in both its frequency and linewidth. This sensitivity is difficult to explain if the mode is assigned solely to a $MnTe_2$ precipitate. (See Note added.)

## IV. PLASMON HYPOTHESIS

If this feature is not a phonon, what origin can it have? There is a Raman-active magnon in this structure [3], but it has a much lower energy and is only observed well below $T_N$. Electronic charge fluctuations (electronic Raman scattering) [28] remain the only plausible candidate.

Electronic Raman scattering is proportional to $-\mathrm{Im}[1/\epsilon(\omega)]$, and in metals the Raman frequency is well below the plasma frequency where this function peaks. Still, even in good metals it is quite observable and routinely used to determine the superconducting gap, for instance. It is

TABLE III. Zone-center optical phonon modes of MnTe in the undistorted $P6_3/mmc$ (No. 194) structure and the $P\bar{6}m2$ (No. 187) structure obtained by freezing in a $B_{1u}$ symmetry-breaking distortion (0.1% displacement along the $c$ axis). R, Raman active; IR, infrared active. The $B_{1u}$ distortion lowers the symmetry and activates previously silent modes.

| Undistorted ($P6_3/mmc$, No. 194) | | | Distorted ($P\bar{6}m2$, No. 187) | | |
|---|---|---|---|---|---|
| $\omega_{\rm ph}$ (cm$^{-1}$) | Mode | Activity | $\omega_{\rm ph}$ (cm$^{-1}$) | Mode | Activity |
| 176.91 | $B_{1u}$ | silent | 176.43 | $A_1'$ | R |
| 126.47 | $E_{1u}$ | IR | 126.29 | $E'$ | R, IR |
| 124.97 | $A_{2u}$ | IR | 124.76 | $A_2''$ | IR |
| 121.74 | $B_{2g}$ | silent | 121.62 | $A_2''$ | IR |
| 91.27 | $E_{2g}$ | R | 91.23 | $E'$ | R, IR |
| 90.13 | $E_{2u}$ | silent | 89.51 | $E''$ | R |

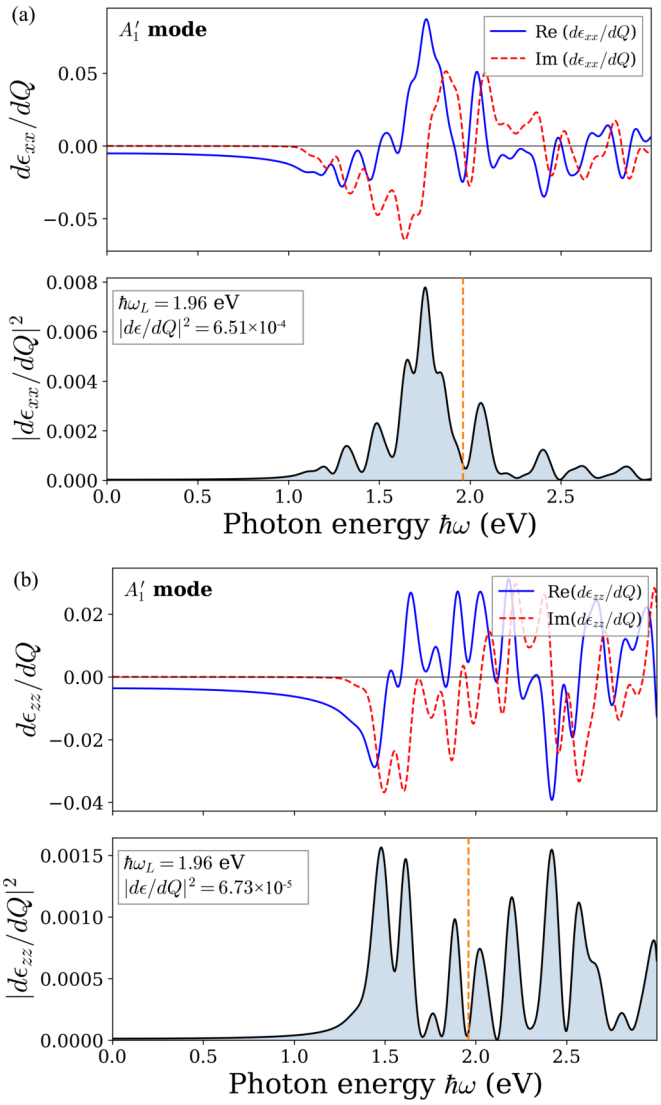


FIG. 2. Dielectric derivatives $d\varepsilon_{\alpha\beta}/dQ$ for the $A_1'$ Raman mode of MnTe ($P\bar{6}m2$, $D_{3h}$). (a) In-plane response $d\varepsilon_{xx}/dQ$. (b) Out-of-plane response $d\varepsilon_{zz}/dQ$. In each panel, the upper subplot shows the real and imaginary parts of $d\varepsilon_{\alpha\beta}/dQ$, while the lower subplot shows $|d\varepsilon_{\alpha\beta}/dQ|^2$, which is proportional to the Raman intensity. By hexagonal symmetry, $\varepsilon_{xx} = \varepsilon_{yy}$; the cross-polarization components vanish for the totally symmetric $A_1'$ mode, consistent with the experimental observation that this mode is active only in parallel ($XX$) polarization geometry. The out-of-plane ($zz$) response is significantly weaker than the in-plane components.

hard to compare the absolute intensities of electronic and phononic Raman scattering in DFT calculations, but it is worth mentioning that, to a good approximation (specifically, resonant effects), the prefactor for the Raman intensity is determined by the fluctuations of the inverse effective mass over the Fermi surface, i.e., $m^{-1}(\mathbf{k}) - \langle m^{-1}\rangle$, where $m^{-1}(\mathbf{k})$ is the second derivative of electron energy with respect to momentum, and $\langle m^{-1}\rangle$ is its average over the Fermi surface [28]. As discussed below, at the relevant doping level several bands with very different effective masses contribute to transport, assuring that the prefactor is not small.

TABLE IV. Comparison of the calculated Raman response $|\partial\varepsilon_{\alpha\beta}/\partial Q|^2$ for the $A_1'$ and $E'$ phonon modes in the distorted $P\bar{6}m2$ structure. The $A_1'$ mode originates from the silent $B_{1u}$ mode and becomes Raman active only due to symmetry breaking, whereas the $E'$ mode descended from $E_{2g}$ is intrinsically Raman active. The dielectric response was evaluated at the incident laser photon energy $\hbar\omega_L = 1.96$ eV ($\lambda = 633$ nm), corresponding to the experimental backscattering Raman configuration. A dash in the last column means that this activity is forbidden by symmetry.

| Mode | Origin | $\omega_{\rm ph}$ (cm$^{-1}$) | $\lvert d\varepsilon_{xx}/dQ\rvert^2$ | $\lvert d\varepsilon_{zz}/dQ\rvert^2$ |
|---|---|---|---|---|
| $A_1'$ | $B_{1u}$ | 176 | $6.51\times10^{-4}$ | $6.7\times10^{-5}$ |
| $E'$ | $E_{1u}$ | 126 | $4.92\times10^{-4}$ | – |
| $E'$ | $E_{2g}$ | 91 | $4.59\times10^{-2}$ | – |
| Ratio ($E'_{91}/A'_1$) | | | ~70 | – |
| Ratio ($E'_{91}/E'_{126}$) | | | ~90 | – |

Let us now estimate the frequency of such plasmon. Pristine MnTe is a $p$-type semiconductor with a typical hole concentration on the order $p \sim 10^{18}$ cm$^{-3}$, or $10^{-4}$ per unit cell (Table II). The bands near the valence band maximum at the $A$ point [29,30] are dominated by the Te $p_x$ and $p_y$ orbital character and well described, in the altermagnetically ordered state, by a four-band $\mathbf{k}\cdot\mathbf{p}$ Hamiltonian including symmetry-allowed spin-orbit coupling (SOC) up to linear order in $k$ [31]. We will use this $\mathbf{k}\cdot\mathbf{p}$ model to describe the transport properties of MnTe. Without SOC, the bands in this model are fourfold degenerate along the $A\Gamma$ direction with the out-of-plane effective mass $m_\perp^* = 1.14m_0$, while the in-plane dispersion exhibits two pairs of degenerate bands: light holes with $m_{lh}^* = 0.13m_0$ and heavy holes with $m_{hh}^* = 0.53m_0$. Spin-orbit coupling lifts the degeneracy at a generic $k$ and induces conical dispersions near the $A$ point. The $A$ point itself remains fourfold degenerate up to a tiny splitting in the order of 1 meV, which may be ignored for our purposes.

The tensor of squared plasma frequency can be calculated directly from the band structure using the standard definition [32]:

$$\left(\omega_p^2\right)_{\alpha\beta} = \varepsilon^{-1}\sum_n \int v_{n\alpha}v_{n\beta}\frac{\partial f(E_n)}{\partial\mu}\frac{d^3k}{(2\pi)^3}, \qquad (3)$$

where $\varepsilon$ is the dielectric constant in the absence of charge carriers, the $\mathbf{v}_n(\mathbf{k})$ and $E_n(\mathbf{k})$ are the group velocity and energy of band $n$, and $f(E_n)$ is the Fermi-Dirac distribution at chemical potential $\mu$. The two independent components of this tensor in hexagonal MnTe are $\omega_{p,xx}^2 = \omega_\parallel^2$ and $\omega_{p,zz}^2 = \omega_\perp^2$. The resulting $\omega_\parallel$ and $\omega_\perp$ are plotted in Fig. 3 as a function of the hole concentration $p$, neglecting semiconducting screening for the moment. Interestingly, despite this being a multiband and not exactly parabolic bands system, $\omega_p^2$ are approximately proportional to the hole concentration. Reported values in Table II cluster around (2–6.8) $\times 10^{18}$ cm$^{-3}$, corresponding in Fig. 3 to $\omega_\parallel \sim$ 500–1000 cm$^{-1}$ and $\omega_\perp \sim$ 350–660 cm$^{-1}$. Now, these should be divided by $\sqrt{\varepsilon(0)}$, the refraction index of undoped MnTe. Our calculations give $\varepsilon_c(0) \approx \varepsilon_{ab}(0) \approx 10$, in agreement with previous calculations and experiments (see Ref. [33], Fig. 4). Thus, we expect the plasmon frequencies to be between 170–320 and 120–220 cm$^{-1}$, respectively, in the ballpark of the observed Raman line. Given a semiquantative character of the estimates above, the plasmon origin is plausible.

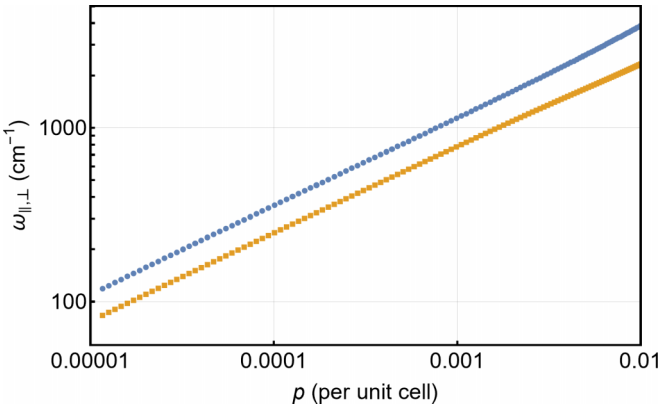


FIG. 3. Plasma frequencies $\omega_\parallel$ (blue circles) and $\omega_\perp$ (orange squares) as a function of the hole concentration $p$ at $T = 150$ K, calculated assuming $\varepsilon = \varepsilon_0$.

The above calculation assumes that transport in MnTe is well described by the band model, which requires that the mean-free path $\lambda$ is at least a few times larger than the interatomic distance. We estimate $\lambda$ using the experimental data on the electric resistivity [34] and the $\mathbf{k} \cdot \mathbf{p}$ band structure.

In the relaxation-time approximation, the in-plane conductivity is $\sigma_\parallel = \varepsilon\omega_\parallel^2\tau$. According to Ref. [34], the resistivity of undoped MnTe samples at $T = 150$ K (which is well below the Néel temperature $T_N$) varies approximately from 0.03 to 3 Ω cm, depending on the heat treatment and crystallographic orientation of the sample. Using our calculated $\sqrt{\varepsilon}\omega_\parallel \approx 360$ cm$^{-1}$, the corresponding range of the relaxation time is $\tau \sim 0.8$–80 fs.

The mean-squared group velocity was found by dividing $\varepsilon\omega_\parallel^2$ from Eq. (3) by the similar density-of-states-like integral without the velocities in the integrand. This results in $\sqrt{\langle v_x^2\rangle} \approx 3.7 \times 10^5$ m/s. The mean-free path can then be estimated as $\lambda = \sqrt{2\langle v_x^2\rangle}\,\tau \sim 0.3$–30 nm.

Thus, with the possible exception of the most resistive samples with $\rho \gtrsim 1$ Ω cm, the mean-free path corresponding to the experimental resistivity exceeds the lattice spacing, supporting the treatment of transport properties within the band model. This conclusion is consistent with the temperature dependence $\rho(T)$ of the resistivity in those samples [34]: those with $\rho < 1$ Ω cm have metallic (monotonically increasing) $\rho(T)$, while those with $\rho > 1$ Ω cm have a minimum at $T \sim 100$ K, suggesting thermally activated carriers with activation energy on the order of 10 meV.

## V. CONCLUSIONS

From our analysis, we arrive at the following conclusions:

(1) The strong Raman-active mode observed at about 175 cm$^{-1}$ and routinely assigned to the $E_{2g}$ phonon [2,4–6] is not the latter (as suggested by Wu *et al.* [7]), and is a Raman excitation of unknown origin.

(2) This excitation, contrary to the conjecture of Ref. [7], is not the forbidden $B_{1u}$ mode that "leaks" because of an intrinsic symmetry lowering.

(3) While an impurity-phase (e.g., $MnTe_2$) phonon origin cannot be rigorously excluded, the presence of an anomaly at the MnTe Néel temperature for this mode is hard to explain in this scenario. On the other hand, a change in the plasmon frequency due to magnetic ordering is naturally expected.

(4) A plausible explanation is that this mode is a plasmon excitation due to hole self-doping, which has the right symmetry (also for the pump-probe coherent excitations in Ref. [9]). There are open questions with this interpretation as well—for instance, why the second plasmon is not visible: too soft? too weak? too broad? However, it is clear from our results that this mode is not an intrinsic phonon, and the doped-hole plasmons have the correct symmetry, and the frequencies in the right range are in the right ballpark.

Final verification of this hypothesis will be provided by future experiments, and can shed new light on the nature of doping and electronic transport (including, but not limited to altermagnetic transport effects) in MnTe.

## VI. EXPERIMENTAL OUTLOOK

Possible experimental tests of the plasmon hypothesis include direct detection of plasmons via energy loss spectroscopy or electronic microscopy, accessing the out-of-plane polarized plasmon, which should appear at a different energy, using the corresponding light polarization, as well as indirect tests using MnTe modified in a way that does not significantly change the phonon properties but does affect the carrier concentration, such as very low-dosage doping with Li.

*Note added.* Recently, we became aware of a work [27] that presented evidence in favor of the extrinsic character of the ∼175 cm$^{-1}$ Raman excitation, whose presence was sample dependent, and its assignment to two closely spaced $A_g$ and $T_g$ modes in the $MnTe_2$ impurity phase. This conclusion is based in part on the absence of the anomaly for these modes at $T_N$ for MnTe and the presence of a weak anomaly near $T_N$ of $MnTe_2$. The absence of an anomaly near $T_N$ of MnTe strongly disagrees with observations of Refs. [5,6]. Also, in contrast to earlier work, Ref. [27] reports two nearby Raman modes—the lower one active only in *XX* polarization (similar to Ref. [7]), but the higher mode having larger intensity in *XY* polarization compared to *XX*. Different properties of the Raman excitations observed in different measurements suggest they may not be attributable to a single origin.

## ACKNOWLEDGMENTS

We acknowledge helpful discussions with Thomas Devereaux, Rudi Hackl, Patrick Vora, Alberto de la Torre, Badih Assaf, Angela Hight-Walker, and Rafaël Hermann. The work at George Mason University was supported by the Army Research Office under Cooperative Agreement No. W911NF-22-2-0173, and that at the University of Nebraska by the U.S. Department of Energy (DOE) Established Program to Stimulate Competitive Research (EPSCoR) through Grant No. DE-SC0024284. Most calculations were performed using resources provided by the Office of Research Computing at George Mason University, funded in part by grants from the National Science Foundation (Award No. 2018631) and utilizing the Holland Computing Center of the University of Nebraska, which receives support from the UNL Office of Research and Innovation, and the Nebraska Research Initiative.

## DATA AVAILABILITY

The data that support the findings of this article are not publicly available upon publication because it is not technically feasible and/or the cost of preparing, depositing, and hosting the data would be prohibitive within the terms of this research project. The data are available from the authors upon reasonable request.


[1] P. Negi, S. S. S. A. Aradhyula, S. Dutta, and S. Roychowdhury, MnTe rising: A modern era of thermoelectric and altermagnetic materials, Chem. Mater. **37**, 6097 (2025).

[2] S. R. Mobasser and T. R. Hart, Raman scattering from phonons and magnons in magnetic semiconductor, MnTe, in *Spectroscopic Characterization Techniques for Semiconductor Technology II*, edited by F. H. Pollak and R. Tsu (SPIE, Bellingham, WA, 1985), Vol. 0524, pp. 137–144.

[3] W. Szuszkiewicz, J. Mohrange, M. Jouanne, M. Kanehisa, R. Swirkowicz, R. E. Dynowska, E. Janik, T. Wojtowicz, and J. Kossut, Temperature dependence of Raman scattering by magnons in bulk-like MBE-grown MnTe films, Acta Phys. Pol. A **92**, 1025 (1997).

[4] W. Szuszkiewicz, M. Jouanne, J.-F. Morhange, M. Kanehisa, E. Dynowska, K. Gas, E. Janik, G. Karczewski, R. Kuna, and T. Wojtowicz, Raman scattering as a tool to characterize semiconductor crystals, thin layers, and low-dimensional structures containing transition metals, Phys. Status Solidi B **251**, 1133 (2014).

[5] J. Zhang, Q. Lian, Z. Pan, W. Bai, J. Yang, Y. Zhang, X. Tang, and J. Chu, Spin-phonon coupling and two-magnons scattering behaviors in hexagonal NiAs-type antiferromagnetic MnTe epitaxial films, J. Raman Spectrosc. **51**, 1383 (2020).

[6] K. P. Kluczyk, K. Gas, M. J. Grzybowski, P. Skupinski, M. A. Borysiewicz, T. Fas, J. Suffczynski, J. Z. Domagala, K. Grasza, A. Mycielski, M. Baj, K. H. Ahn, K. Vyborny, M. Sawicki, and M. Gryglas-Borysiewicz, Coexistence of anomalous Hall effect and weak magnetization in a nominally collinear antiferromagnet MnTe, Phys. Rev. B **110**, 155201 (2024).

[7] A. Wu, D. Cheng, X. Wang, M. Zeng, C. Liu, and X. Li, Optical signatures of noncentrosymmetric structural distortion in altermagnetic MnTe, arXiv:2503.17742.

[8] M. I. Aroyo, J. M. Perez-Mato, C. Capillas, E. Kroumova, S. Ivantchev, G. Madariaga, A. Kirov, and H. Wondratschek, Bilbao crystallographic server: I. Databases and crystallographic computing programs, Z. Kristallogr.-Cryst. Mater. **221**, 15 (2006).

[9] D. Bossini, S. Dal Conte, M. Terschanski, G. Springholz, A. Bonanni, K. Deltenre, F. Anders, G. S. Uhrig, G. Cerullo, and M. Cinchetti, Femtosecond phononic coupling to both spins and charges in a room-temperature antiferromagnetic semiconductor, Phys. Rev. B **104**, 224424 (2021).

[10] H. J. Zeiger, J. Vidal, T. K. Cheng, E. P. Ippen, G. Dresselhaus, and M. S. Dresselhaus, Theory for displacive excitation of coherent phonons, Phys. Rev. B **45**, 768 (1992).

[11] M. Walter and M. Moseler, *Ab initio* wavelength-dependent Raman spectra: Placzek approximation and beyond, J. Chem. Theory Comput. **16**, 576 (2020).

[12] J. Wasscher and C. Haas, Contribution of magnon-drag to the thermoelectric power of antiferromagnetic Mn Te, Phys. Lett. **8**, 302 (1964).

[13] W. Xie, S. Populoh, K. Galazka, X. Xiao, L. Sagarna, Y. Liu, M. Trottmann, J. He, and A. Weidenkaff, Thermoelectric study of crossroads material MnTe via sulfur doping, J. Appl. Phys. **115**, 103707 (2014).

[14] Y. Ren, Q. Jiang, J. Yang, Y. Luo, D. Zhang, Y. Cheng, and Z. Zhou, Enhanced thermoelectric performance of MnTe via Cu doping with optimized carrier concentration, J. Materiomics **2**, 172 (2016), Special Issue on Advances in Thermoelectric Research.

[15] S. Zulkifal, S. Siddique, Z. Wang, X. Zhang, X. Huang, Q. Xia, Q. Zhang, S. Li, P. Wang, D. Li, P. Ying, Y. Zhang, and G. Tang, All-scale hierarchical structuring, optimized carrier concentration, and band manipulation lead to ultra-high thermoelectric performance in eco-friendly MnTe, Small **20**, 2310123 (2024).

[16] Y. Xu, W. Li, C. Wang, J. Li, Z. Chen, S. Lin, Y. Chen, and Y. Pei, Performance optimization and single parabolic band behavior of thermoelectric MnTe, J. Mater. Chem. A **5**, 19143 (2017).

[17] D. Kriegner, K. Výborný, K. Olejník, H. Reichlová, V. Novák, X. Marti, J. Gazquez, V. Saidl, P. Němec, V. V. Volobuev, G. Springholz, V. Holý, and T. Jungwirth, Multiple-stable anisotropic magnetoresistance memory in antiferromagnetic MnTe, Nat. Commun. **7**, 11623 (2016).

[18] M. Cardona, *Light Scattering in Solids I: Introductory Concepts* (Springer Science & Business Media, Berlin, 2005), Vol. 8.

[19] G. Kresse and J. Hafner, *Ab initio* molecular dynamics for liquid metals, Phys. Rev. B **47**, 558 (1993).

[20] G. Kresse and J. Furthmüller, Efficiency of *ab-initio* total energy calculations for metals and semiconductors using a plane-wave basis set, Comput. Mater. Sci. **6**, 15 (1996).

[21] G. Kresse and J. Furthmüller, Efficient iterative schemes for *ab initio* total-energy calculations using a plane-wave basis set, Phys. Rev. B **54**, 11169 (1996).

[22] J. P. Perdew, K. Burke, and M. Ernzerhof, Generalized gradient approximation made simple, Phys. Rev. Lett. **77**, 3865 (1996).

[23] H. Stokes, D. Hatch, and B. Campbell, SMODES, ISOTROPY software suite (2021).

[24] H. T. Stokes and D. M. Hatch, FINDSYM: Program for identifying the space-group symmetry of a crystal (2005).

[25] T. Bohm, R. Hackl, *et al.* (unpublished).

[26] A. E. Fahmy, A. J. Williams, Y. Li, T. T. Mai, K. F. Garrity, M. B. Stone, M. J. Karaki, S. Haravifard, A. R. H. Walker, R. V. Aguilar, J. E. Goldberger, and Y.-M. Lu, Weyl magnons in the non-coplanar antiferromagnet $MnTe_2$, arXiv:2512.18534.

[27] E. Uykur, M. V. Gonçalves-Faria, S. Rößler, V. A. Ginga, M. Schmidt, S. Winnerl, M. Helm, and A. A. Tsirlin, Revisiting the symmetry and optical phonons of altermagnetic $\alpha$-MnTe, Phys. Rev. B **113**, 224107 (2026).

[28] T. P. Devereaux and R. Hackl, Inelastic light scattering from correlated electrons, Rev. Mod. Phys. **79**, 175 (2007).

[29] T. Osumi, S. Souma, T. Aoyama, K. Yamauchi, A. Honma, K. Nakayama, T. Takahashi, K. Ohgushi, and T. Sato, Observation of a giant band splitting in altermagnetic MnTe, Phys. Rev. B **109**, 115102 (2024).

[30] P. E. Faria, Jr., K. A. de Mare, K. Zollner, K.-H. Ahn, S. I. Erlingsson, M. van Schilfgaarde, and K. Výborný, Sensitivity of

the MnTe valence band to the orientation of magnetic moments, Phys. Rev. B **107**, L100417 (2023).

[31] K. D. Belashchenko, Giant strain-induced spin splitting effect in MnTe, a *g*-wave altermagnetic semiconductor, Phys. Rev. Lett. **134**, 086701 (2025).

[32] P. B. Allen, Fermi-surface harmonics: A general method for nonspherical problems. Application to Boltzmann and Eliashberg equations, Phys. Rev. B **13**, 1416 (1976).

[33] H. Sano, M. Kuwahara, H. Kawashima, H. Tsuda, G. Mizutani, and T. An, Optical properties change due to the displacive transition of MnTe and its application to phase-change optical switches, Jpn. J. Appl. Phys. **64**, 102005 (2025).

[34] J. Wasscher, Electrical transport phenomena in MnTe, an antiferromagnetic semiconductor, Ph.D. thesis, Technische Hogeschool Eindhoven, 1969.